

**Stephen J Schiller, Ph.D.**  
**Lead Calibration Scientist**  
**NASA IRIS Co-Principal Investigator**  
[stephen.j.schiller@rtx.com](mailto:stephen.j.schiller@rtx.com)  
 626-664-5577

**Jeffery J. Puschell, Ph.D.**  
**Principal Engineering Fellow**  
**NASA IRIS Principal Investigator**  
[jjpuschell@rtx.com](mailto:jjpuschell@rtx.com)  
 310-503-3412, 805-637-1362

Raytheon Intelligence & Space, 2000 East El Segundo Blvd., El Segundo, CA, USA 90245

# Integrating On-board and Vicarious Calibration with the Improved Radiometric Calibration of Land Imaging Systems (IRIS)



**Space Dynamics Laboratory**  
**Bennett Laboratory building**  
**489 East Innovation Avenue**  
**North Logan UT 84341 USA**

**Tuesday, September 13, 2022 | 4:20 p.m.**

# Meeting the goals of SLI-T

Since 2014, the Sustainable Land Imaging-Technology (SLI-T) Reference Mission Architecture has been the primary design initiative by NASA and USGS for future land imaging.

The resulting technology emerging from the NASA SLI-T program, with the objective of reducing risk, cost, size, volume, mass, and development time for the next generation SLI instruments, has brought about significant innovation from sensor providers supporting the land imaging community.

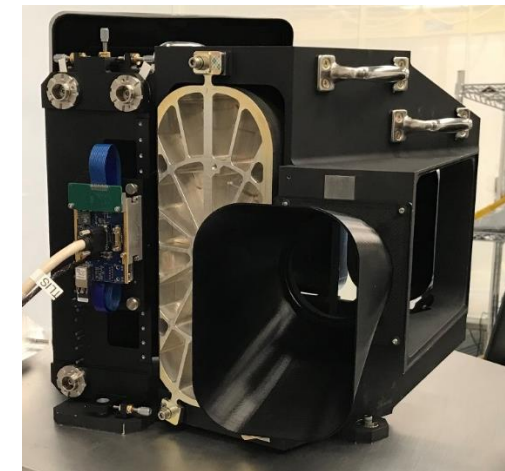
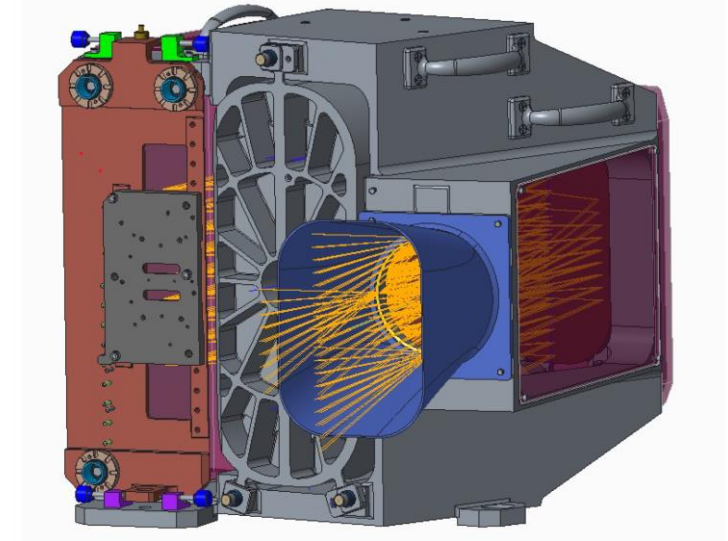
Within Raytheon, this effort led to the development of the ATLIS-prototype imaging system providing VNIR and SWIR focal plane technology and performance validation in support of the NASA and USGS SLI-T goals.

## **The ATLIS-P telescope was the first complete free form reflective triplet operating in the VNIR spectral range and built by US industry**

Surfaces on each telescope mirror are defined using a superposition of Zernike polynomials that can be constructed to correct aberrations, then machined automatically into the mirror surfaces, polished to surface roughness of 2 nm or better and manually assembled and aligned into a telescope with RMS wave front errors of 60 nm or better across the full FOV

The need for larger spherical mirrors is negated, ultimately yielding a significantly smaller, more precise instrument.

Without sacrificing capability, the ATLIS-P design reduced size, weight and power by more than 30 percent compared to the Landsat OLI design



Jeffery J. Puschell, John B. Schlaerth, "Advanced technology land imaging spectroradiometer: a next generation sustainable land imager," Proc. SPIE 10780, Multispectral, Hyperspectral, and Ultraspectral Remote Sensing Technology, Techniques and Applications VII, 1078009 (23 October 2018); doi: 10.1117/12.2501986. Also paper 12236-6 from this conference.

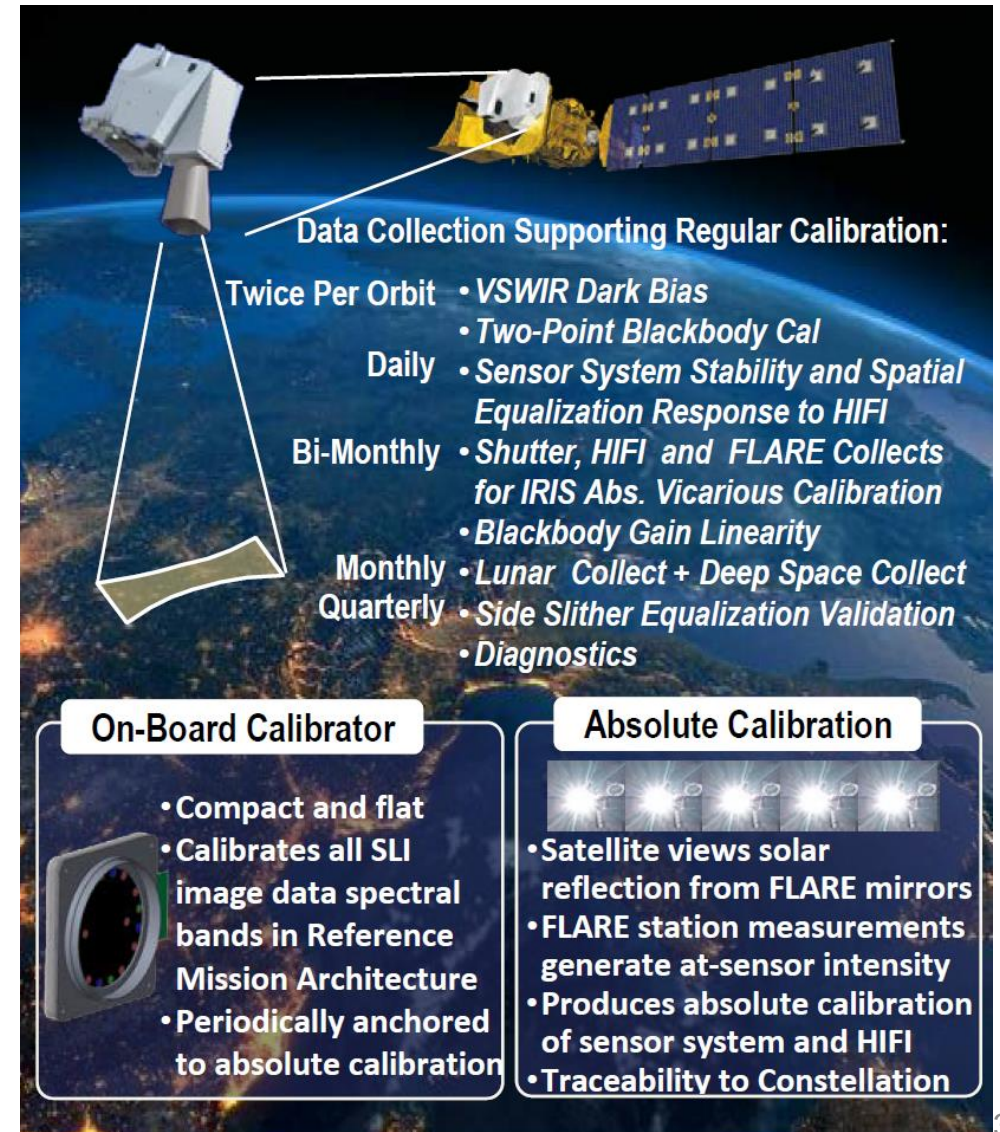
# Emergence of the Improved Radiometric Calibration of Land Imaging Systems (IRIS) program

The ATLAS-P hardware also becomes the testbed for NASA and Raytheon funded demonstrations of calibration as well.

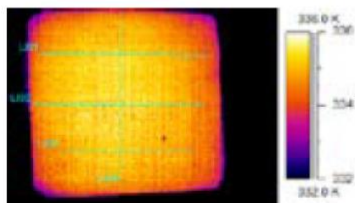
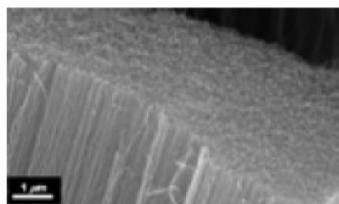
The goal is to pursue further the SLI-T objective of reducing risk, cost, size, volume, and mass, this time as applied to the on-board calibration system.

IRIS involves developing a compact, full spectrum, end-to-end onboard source in which the VSWIR component can be calibrated on-orbit in radiance by repeated observations of high altitude mirrors reflecting the sun toward the imager utilizing the SPARC vicarious calibration method based on Labsphere's FLARE target system.

The IRIS vicarious calibration methodology presented is known as IRIS-V



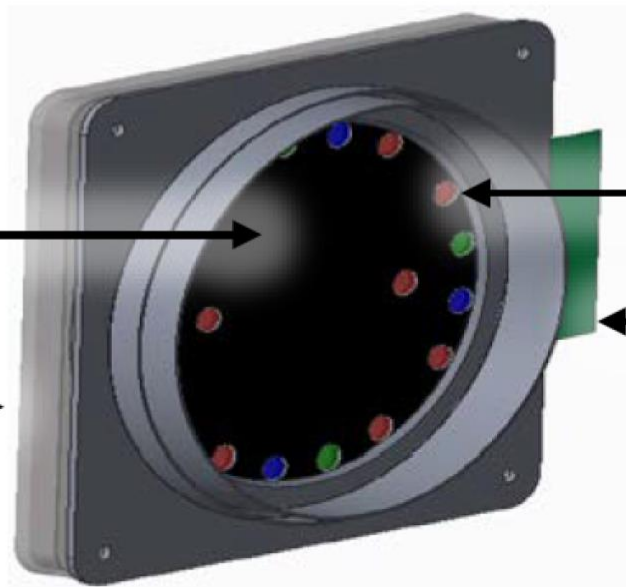
# Flat Panel Full Spectrum Calibrator



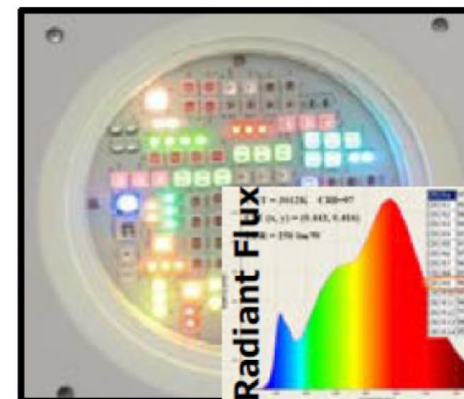
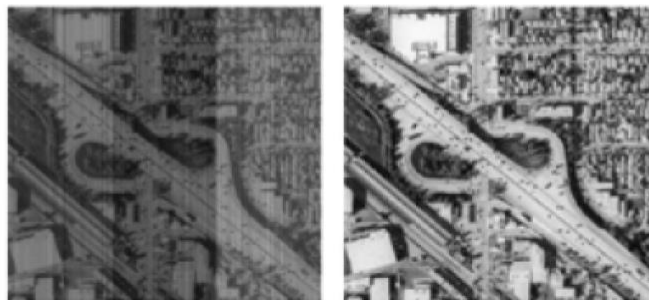
**Blackbody.** Vertically Aligned Carbon Nanotube (VACNT) Blackbody surface provides >99.5% emittance



**Spreader.** <1mm thick multilayered thermal spreader improves uniformity and reduces stabilization time



Before / After Correction



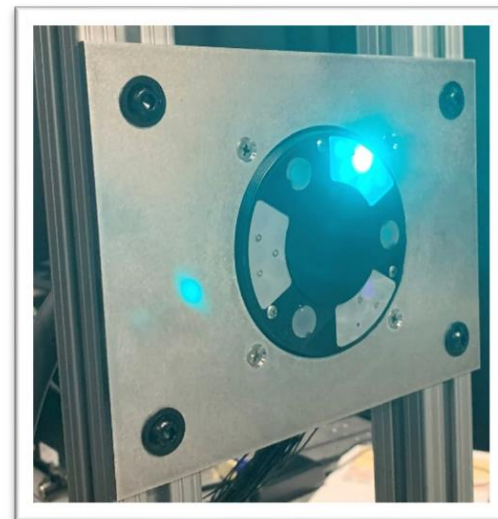
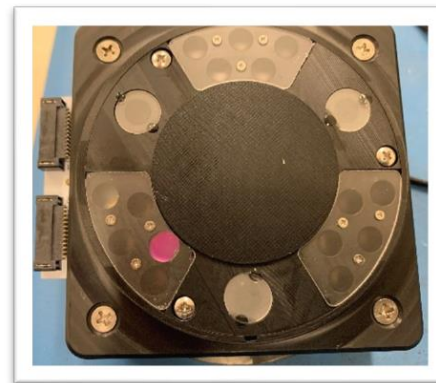
**VSWIR Emitters.** Engineered phosphors enable custom LED spectra



**Articulation.** Compact calibrator articulates into the pupil, enabling calibration of the entire optical path

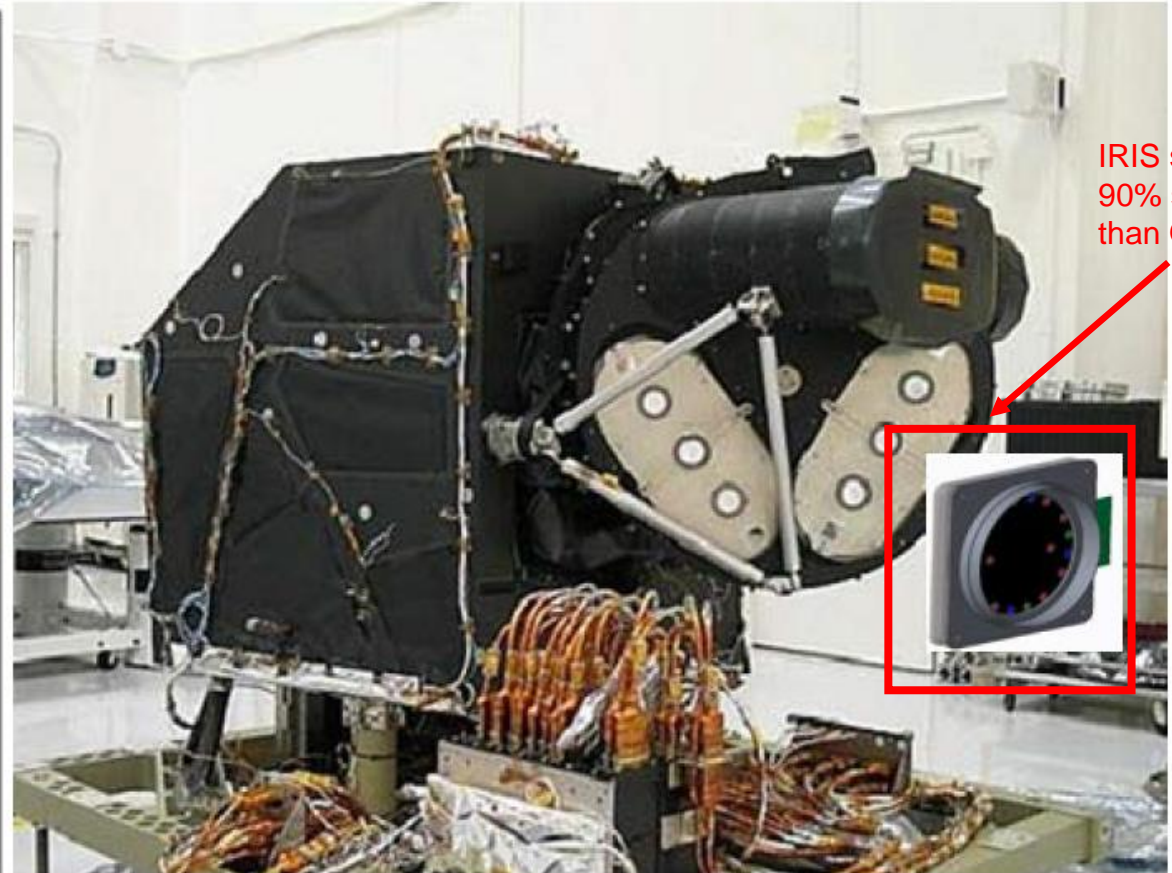
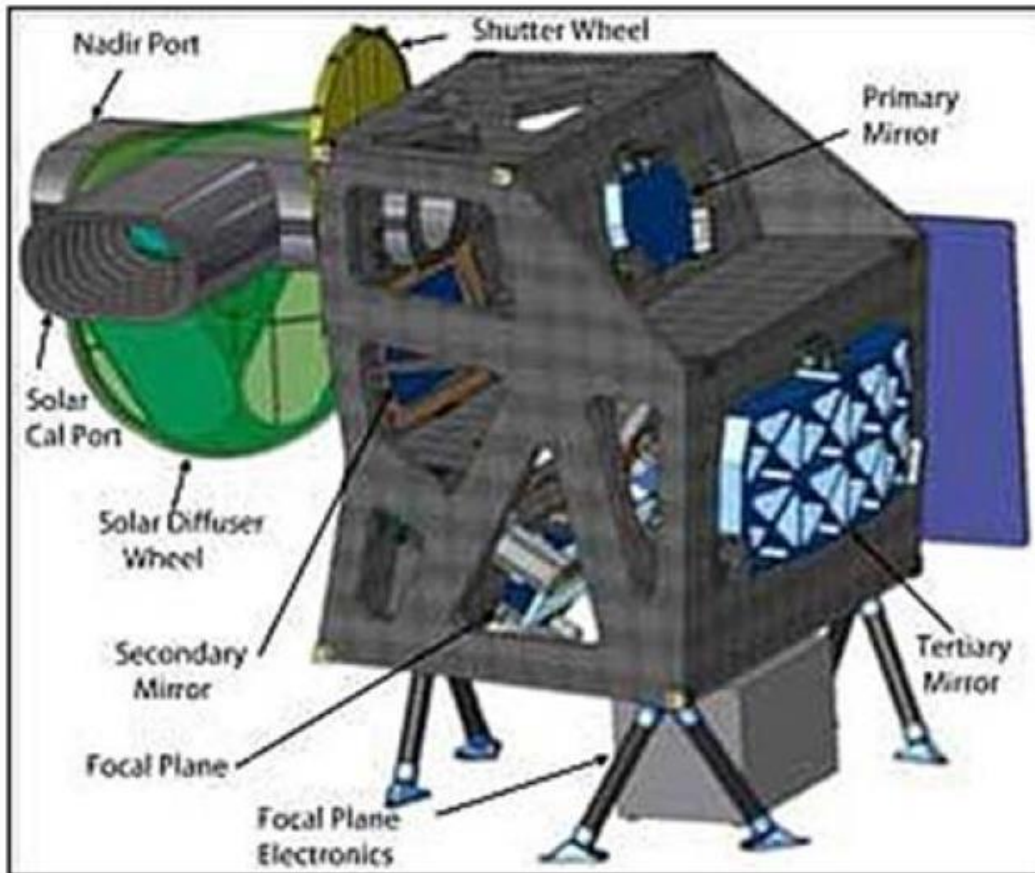
# Jones source characteristics for RMA spectral bands

| Requirements |      |     |       |       |   | Devices Used |      |     |      |      |  |
|--------------|------|-----|-------|-------|---|--------------|------|-----|------|------|--|
| Band         | CWL  | BW  | Low   | High  | In Band Radiant Intensity Specification | Power        | CWL  | BW  | Low  | High | Measured Average In-band Intensity over +/-10° |
|              | nm   | nm  | nm    | nm    | mW/sr                                   | mW           | nm   | nm  | nm   | nm   | mw/sr  |
| 1a           | 410  | 20  | 400   | 420   | 16.3                                    | 710          | 405  | 14  | 398  | 412  | 926.4  |
| 1            | 443  | 20  | 433   | 453   | 18.6                                    | 480          | 450  | 20  | 440  | 460  | 168.4  |
| 2            | 490  | 65  | 457.5 | 522.5 | 60                                      | 240          | 490  | 26  | 477  | 503  | 830.9  |
| 3            | 560  | 35  | 542.5 | 577.5 | 32.3                                    | 280          | 450  | 600 | 400  | 1000 | 34.2   |
| 4a           | 620  | 20  | 610   | 630   | 16.3                                    | 190          | 620  | 15  | 613  | 628  | 194.7  |
| 4            | 665  | 30  | 650   | 680   | 23.4                                    | 250          | 660  | 17  | 652  | 669  | 478.6  |
| 5            | 705  | 15  | 697.5 | 712.5 | 8.1                                     | 250          | 700  | 17  | 692  | 709  | 331.1  |
| 6            | 740  | 15  | 732.5 | 747.5 | 7.4                                     | 320          | 740  | 22  | 729  | 751  | 524.3  |
| 7            | 783  | 20  | 773   | 793   | 9.7                                     | 500          | 780  | 24  | 768  | 792  | 316.2  |
| 8            | 842  | 115 | 784.5 | 899.5 | 85.4                                    | 1400         | 850  | 37  | 832  | 869  | 1201.6   |
| 8a           | 865  | 20  | 855   | 875   | 7.6                                     | 440          | 870  | 50  | 845  | 895  | 159.2  |
| 9            | 945  | 20  | 935   | 955   | 1.3                                     | 1300         | 940  | 47  | 917  | 964  | 212.5  |
| 8b           | 1035 | 20  | 1025  | 1045  | 0.21                                    | 350          | 1050 | 50  | 1025 | 1075 | 331.9  |
| 10           | 1375 | 30  | 1360  | 1390  | 0.65                                    | 17           | 1450 | 90  | 1405 | 1495 | 12.4   |
| 11           | 1610 | 90  | 1565  | 1655  | 1.3                                     | 16           | 1650 | 120 | 1590 | 1710 | 24.9   |
| 12a          | 2040 | 30  | 2025  | 2055  | 0.44                                    | 15           | 2040 | 80  | 2000 | 2080 | 8.4  |
| 12b          | 2100 | 40  | 2080  | 2120  | 0.52                                    | 15           | 2100 | 80  | 2060 | 2140 | 7.0  |
| 12c          | 2210 | 40  | 2190  | 2230  | 0.44                                    | 15           | 2210 | 80  | 2170 | 2250 | 10.5   |



IRIS breadboard sources exceed requirements in all spectral bands – parts availability issues created challenges at 560 nm that were overcome successfully

# IRIS offers inflight absolute calibration with an on-board system at greatly reduced size, mass and complexity than legacy systems

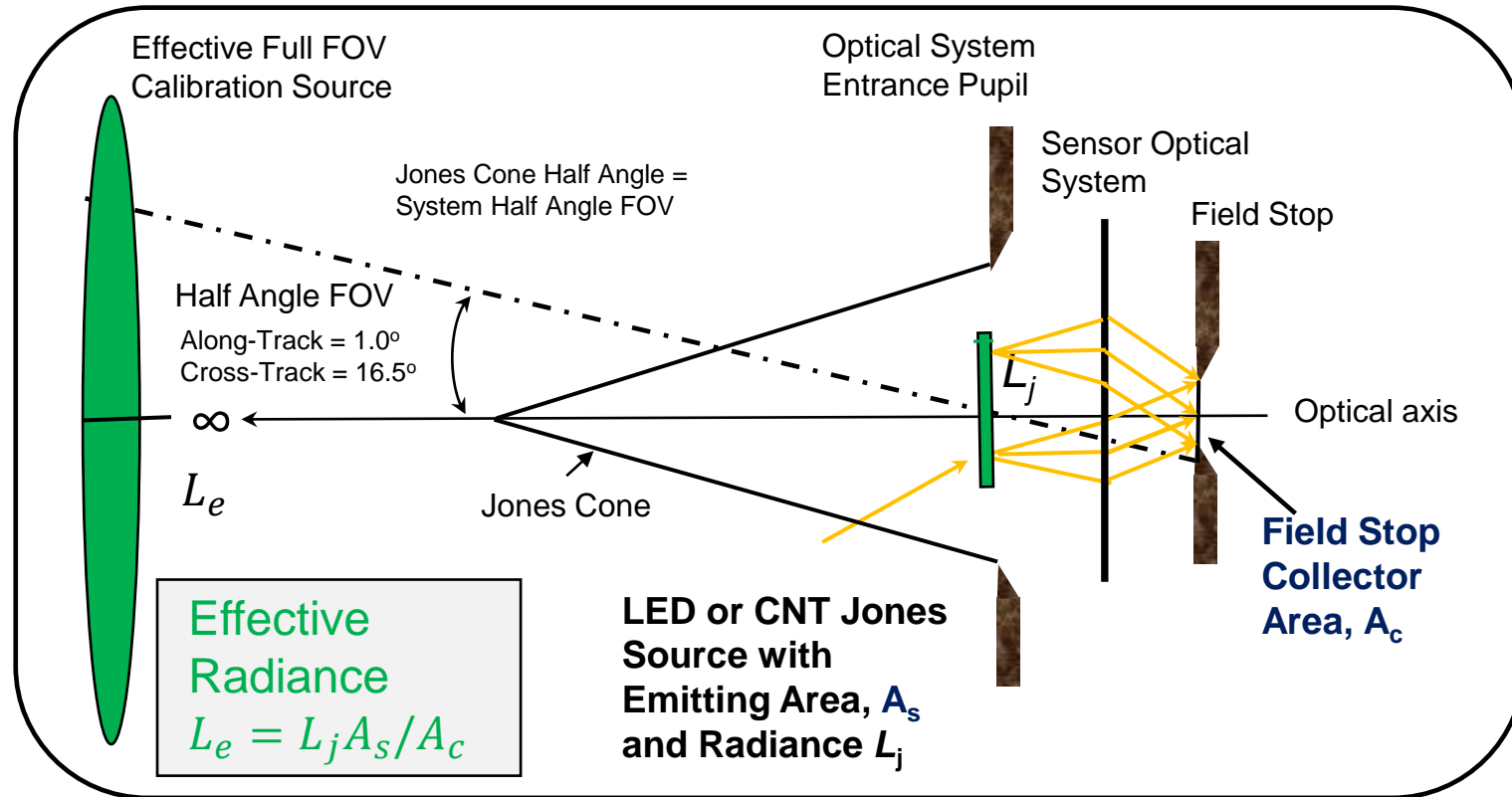


Drawing from: Markham, Brian L., and Julia A. Barsi. "Landsat-8 operational land imager on-orbit radiometric calibration." *2017 IEEE International Geoscience and Remote Sensing Symposium (IGARSS)*. IEEE, 2017.

# Onboard calibration design utilizes the Jones source method providing uniform illumination from sub-aperture sources

## Properties of a Near Field Small Area Jones Source

- Source is small with respect to area of the real Entrance Pupil
- Source is contained entirely with the Jones cone defined by the width of entrance pupil and the system Field-of-View (FOV)
- Under these conditions each point location on the Jones source, emitting rays within the sensor FOV, uniformly illuminates each detector at the field stop
- It is assumed that the only source of radiative energy within the FOV is from the Jones source. Any other light reaching the field stop within the FOV would be stray light, biasing the calibration
- The exact location of the Jones source relative to the entrance pupil does not need to be exactly known as long as it fully lies within the Jones cone.

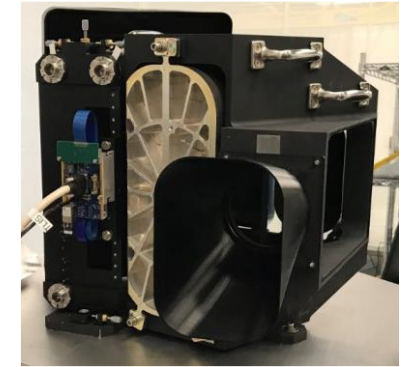


The effective radiance at the focal plane is defined by the emitting area of the Jones Source,  $A_s$ .

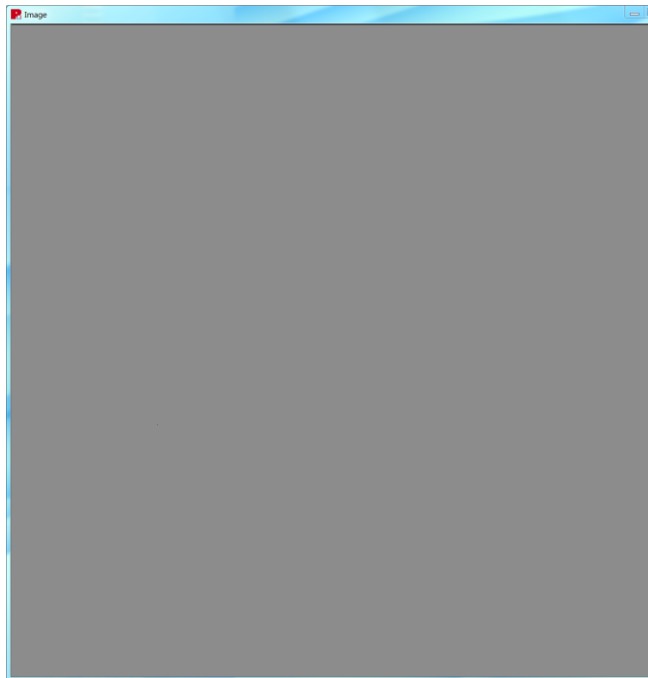
# Jones source calibrator – uniformity demonstration

Jones Source Testing validating uniformity across 2D FPAs

Illustration show actual image recorded by Raytheon’s ATLAS-P imager using the Improved Radiometric Calibration of Land Imaging Systems (IRIS) LED Jones Source.



ATLAS Raw 2k x 2k FPA Image Response from Small Near Field Jones Source

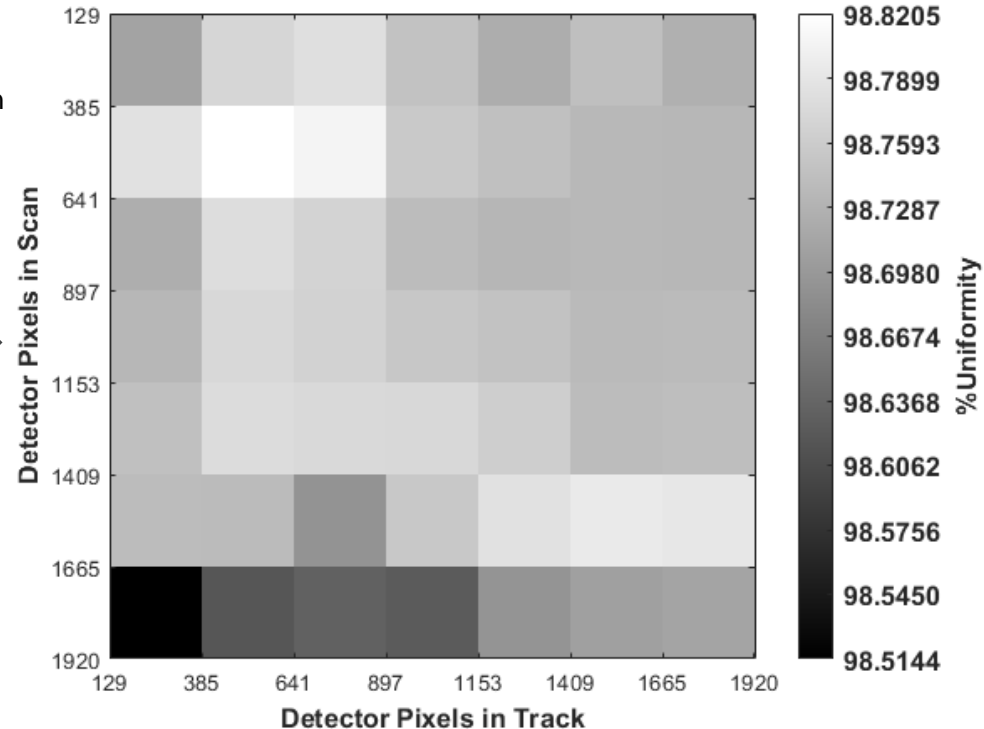


Uniformity coefficient within a partition =  $1 - (\text{stdev}/\text{mean})$  from DN values



The image is not flat field corrected to normalize the detector gains

Partitioned IRIS Image Uniformity at 458nm



Digital number (DN) variations averaged in each partition

Max/min bias spatial variation in the overall partition mean is <0.3% across the full FPA field stop

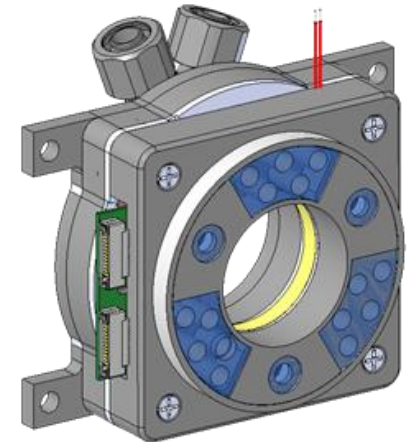
Testing of a 458 nm LED Jones source demo shows only a 0.3% nonuniformity in the partition means across FPA illustrating the Jones Source uniformity performance



# Using IRIS-V vicarious calibration to transfer traceability to the on-board calibrator in-flight

- FLARE allows the sensor to directly view the sun as a metrology irradiance standard in the post-launch environment and provide SI traceability to the sensor land and coastal measurements of radiance and reflectance
- **Goal of IRIS-V is to provide a vicarious method for a near coincident direct comparison of the FLARE measured absolute gain and on-board lamp reference response**
- **The sensor itself then becomes a transfer radiometer establishing a vicarious in-flight SI radiance traceability to the on-board lamp calibration system**
- Repeating the process maintains absolute radiometric knowledge of an on-board lamp source, such as the IRIS ultra-compact HIFI LED calibrator, through its mission lifetime
- The traceability to FLARE worldwide network also supports intersensor calibration and advanced product generation for Landsat data exploitation

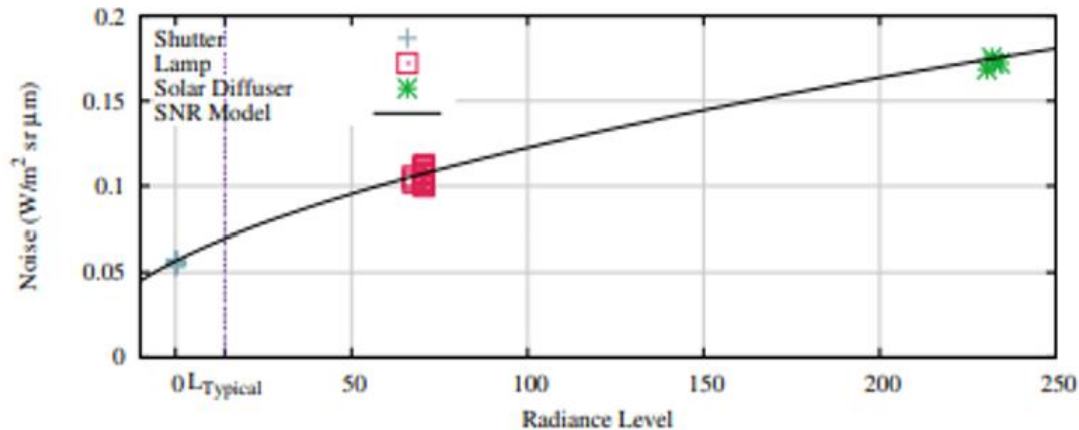
IRIS-V is designed to reduce risk in the application of the IRIS on-board calibrator for future Landsat missions



IRIS HIFI Test System

# Example of the need for using the lamp source absolute radiance response

The Landsat Image Assessment System (IAS) noise model converts the detector mean DN response from lamp illumination to absolute radiance using the gain coefficient derived by the solar calibrator.



**These noise levels are converted from DN to radiance units (W/(m<sup>2</sup> sr μm)) using the band averaged absolute gains from the Calibration Parameter File (solar calibration).**

As is done in IAS processing, a radiance can be derived for the OLI cal lamp assembly illumination via the solar calibrator derived gain coefficient, but the on-board process on it's own is not a metrologically traceable to SI units.

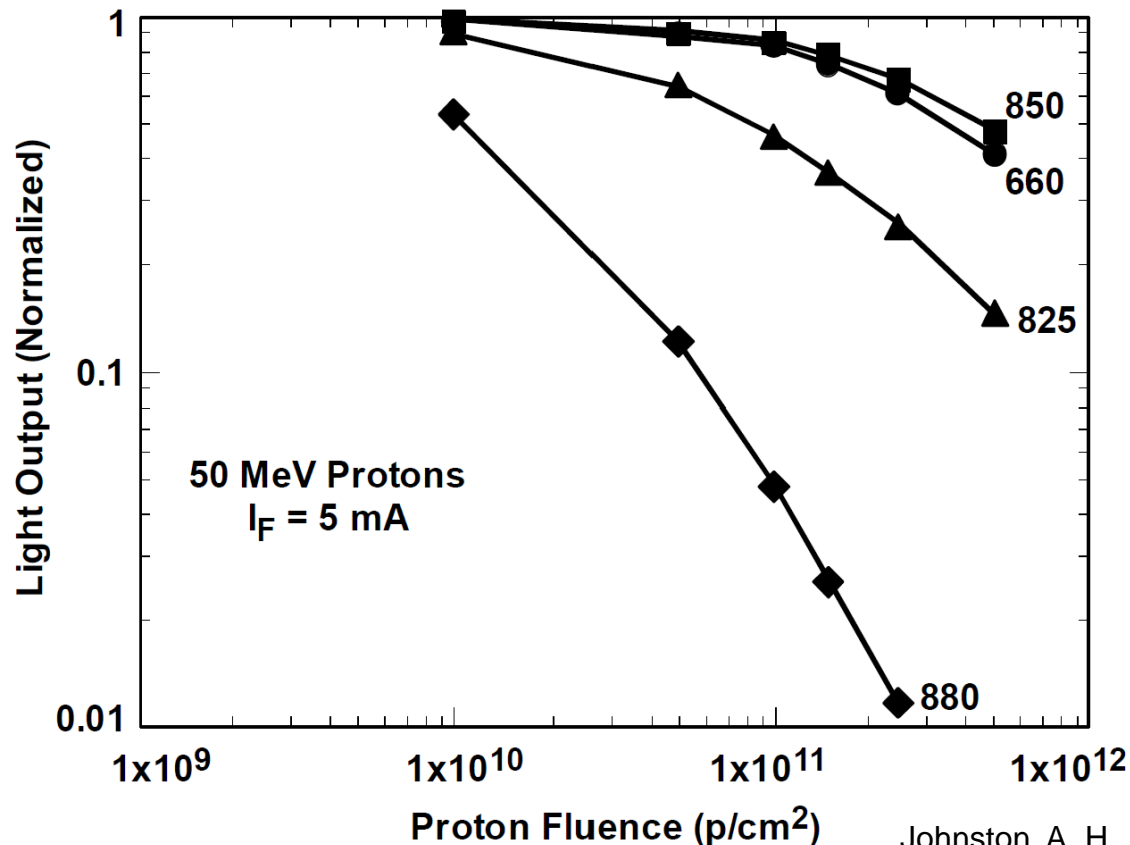
As a result, the solar diffuser derived gain coefficients may include an unknown bias introduced during launch or life on orbit.

Vicarious methods provides a means to insert a traceability path for validation and quantify the bias if present.

# Degradation of LED source output by radiation

IRIS-V provides risk reduction in the operational use of the compact IRIS on-board calibration system

Degradation of LEDs of different wavelengths from 50 MeV protons



Even though LED outputs do not degrade by the same physical processes incandescent lamps do, LEDs can degrade on orbit because of potential radiation effects.

Resistant to gamma radiation (<2% change over 20 years) LEDs and nanomaterials comprising the calibration source may degrade on-orbit significantly due to alpha and beta radiation.

A process for mitigating calibration knowledge errors due to contamination degradation in on-board lamp calibration sources is the main objective of IRIS-V.

Johnston, A. H., et al. "Proton degradation of light-emitting diodes." IEEE Transactions on Nuclear Science 46.6 (1999): 1781-1789.

# IRIS-V demo using FLARE calibrations of Landsat 8 and 9

Performance of IRIS-V is being tested as applied to the L8 and L9 lamp calibration subsystem

This component of the IRIS study is proceeding using FLARE absolute calibrations from

1. FLARE applied to the L8 at the FLARE CONUS nodes using operational vicarious collects underway by Labsphere at the
  - Alpha site, Brookings, SD
  - Beta site, Brock, TexasFLARE vicarious calibration collections of Landsat 8 and 9 have built a two year archive
2. In the future, FLARE operating at Mauna Loa Observatory as a premier vicarious calibration site for the application of the IRIS-V inflight absolute calibration of on-board sources

FLARE gain calibrations of Landsat 8 and 9 are being applied to their on-board lamp source to establish absolute radiance illuminating the focal plane by the lamp source

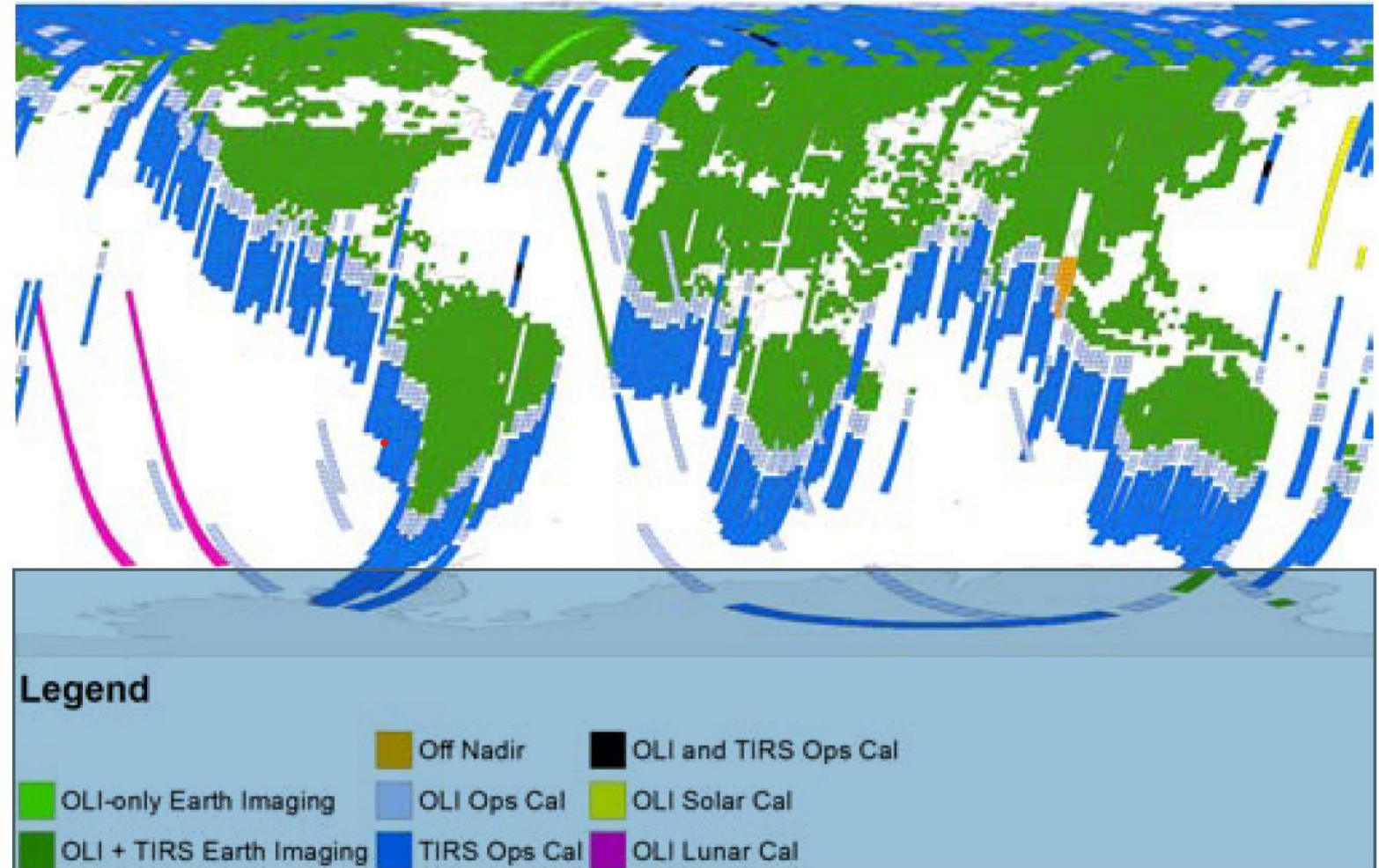
Results will demonstrate the IRIS-V capability to maintain an on-board calibrator's absolute radiance knowledge when applied to future Landsat missions

# How IRIS-V creates a near coincident lamp and vicarious data collect

This diagram presents a representation of global image collection and calibration opportunities within the WRS-2 grid during the 16-day repeat cycle of Landsat 8.

There are many orbits shown (gray and blue paths and white areas) in which on-board calibration has time to proceed over deep ocean without interrupting land collects.

**The IRIS-V calibration process utilizes one of these paths to create an opportunity for a near-coincident on-board lamp and vicarious calibration event.**



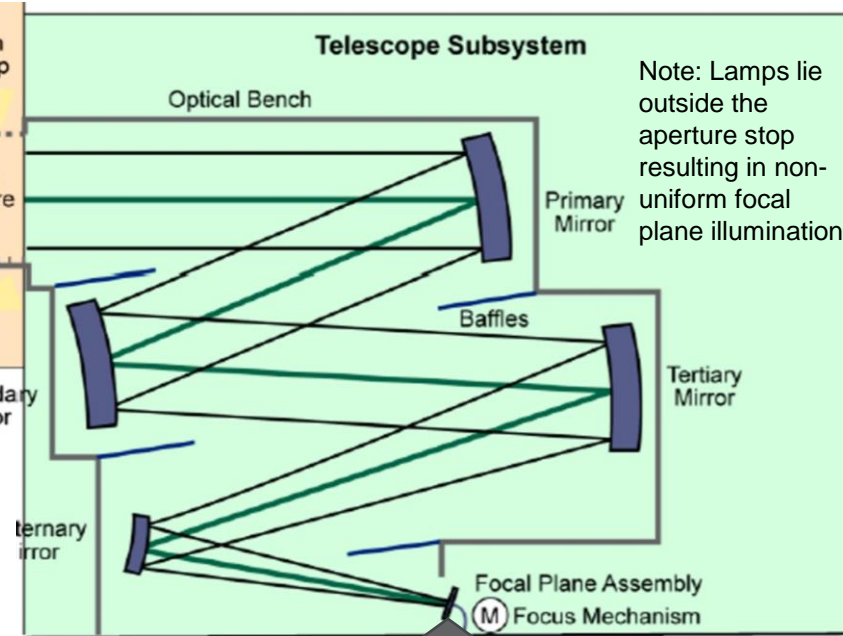
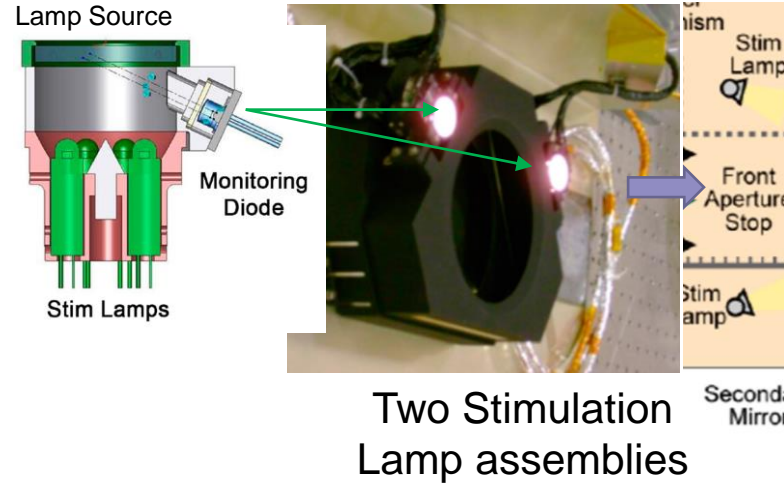
Nelson, James, et al. "Landsat data continuity mission (LDCM) space to ground mission data architecture." *2012 IEEE Aerospace Conference*. IEEE, 2012.

# Is there time over the ocean for a lamp collect

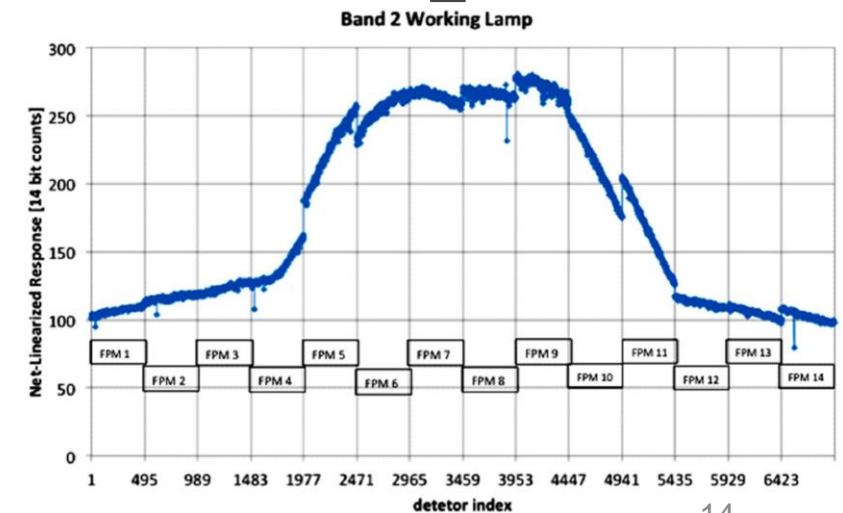
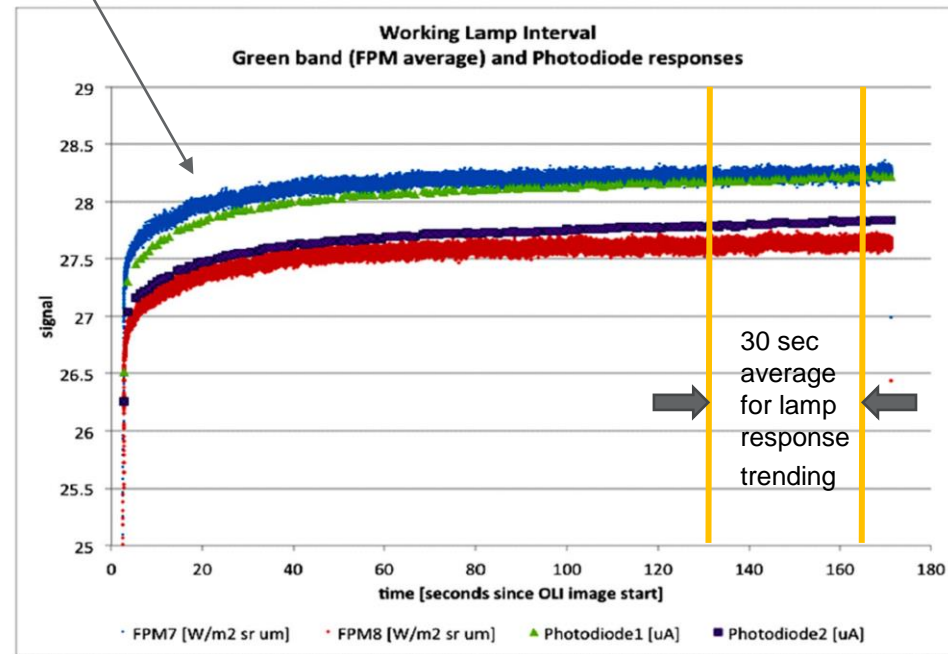
Landsat 8 on-orbit lamp timeline

1. Land imaging end
  2. Close shutter & rest (20 sec)
  3. Take dark measurement (2 sec)
  4. Start lamp data acquisition (2.75 min)
    1. Warm up for 2.2 min
    2. Average DNs for 30 sec
  5. Turn off lamp & rest
  6. Take dark measurement (2 sec)
  7. Shutter Open & rest (20 sec)
  8. Land imaging restart
- Min. Time: 4 min 17 sec**  
 (timing information provided by USGS EROS CalVal Team)

The IRIS HIFI system  
**Time < 2 min**



Note: Lamps lie outside the aperture stop resulting in non-uniform focal plane illumination



# Deployment on the Big Island of Hawaii provides an ideal site for IRIS-V

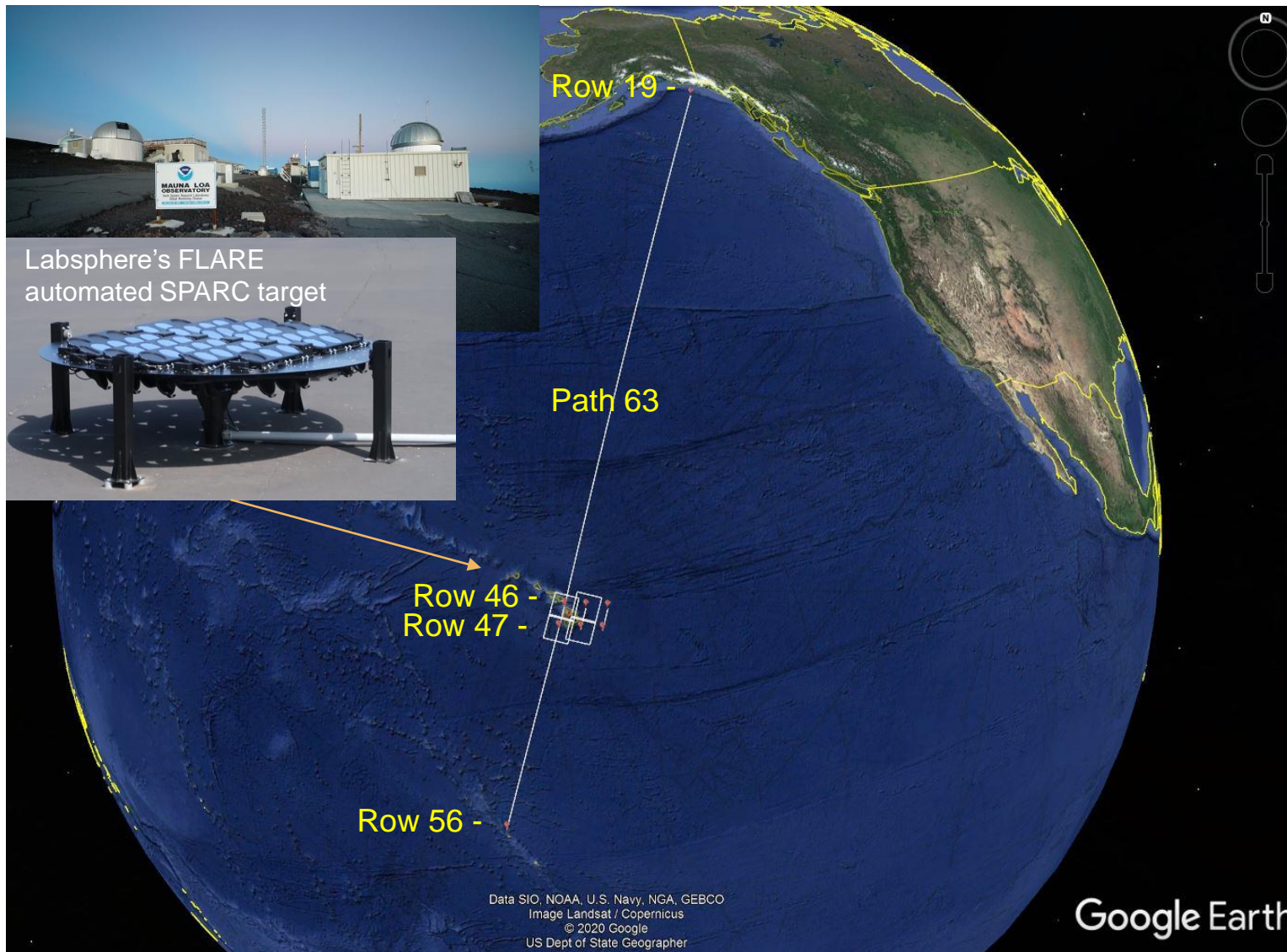


Illustration shows the opportunity in path 63 over deep ocean for which Landsat 8 is idle in collecting imagery of the Earth

It is during this part of the orbit in which images of the on-board lamp illumination and the dark shutter can be collected

Only earth views in Rows 46 and 47 are processed over the orbital path from Rows 19 to 56 for example

Time is available for an IRIS lamp and shutter collect on approach to the location of a Mauna Loa FLARE calibration target without interrupting land imaging

The near coincidence transfers absolute performance knowledge from the vicarious calibration event to the on-board lamp without time for significant relative bias or gain drift, maintaining traceability

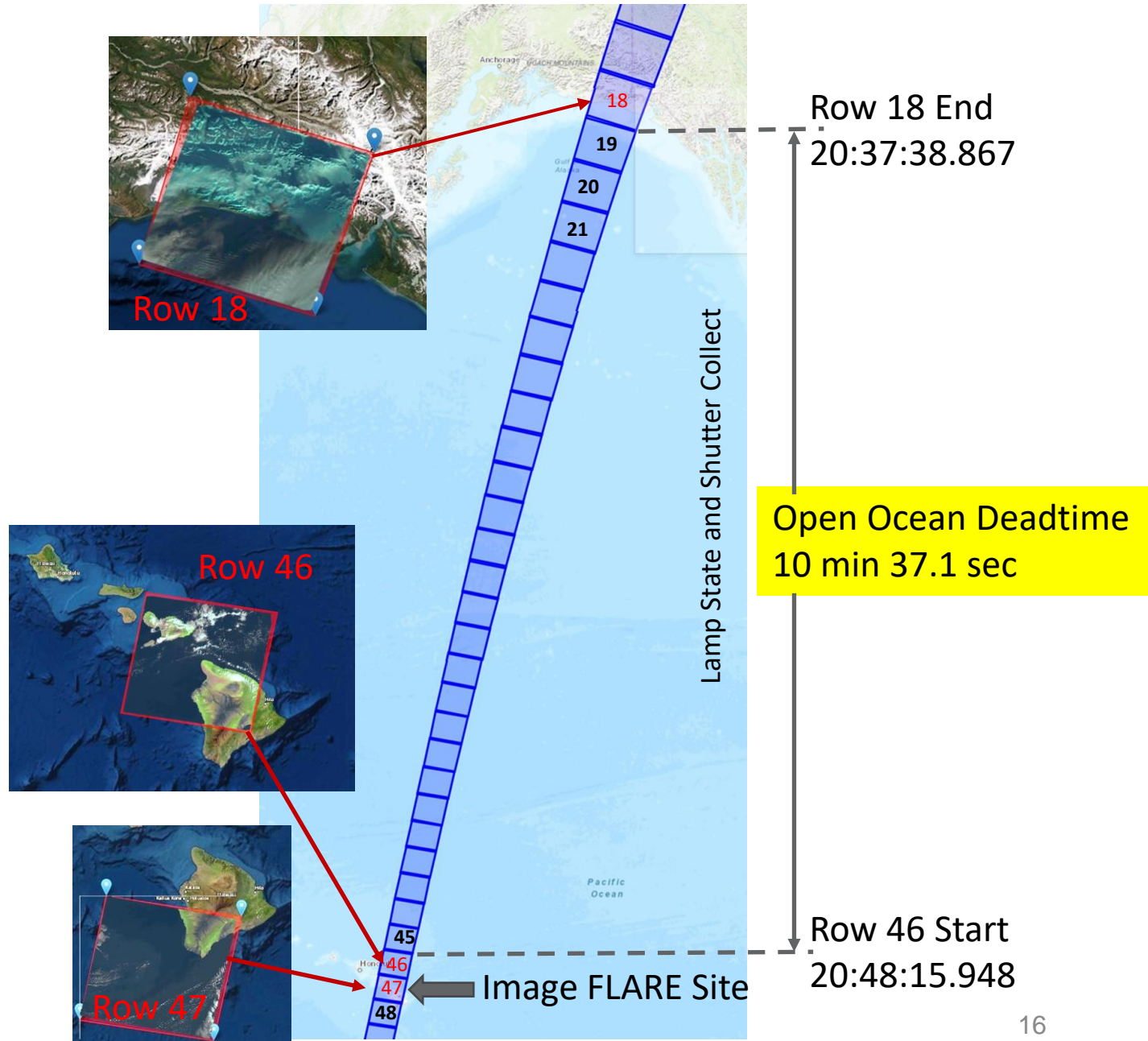
This is the orbital component for the methodology of IRIS-V

# Descending Path 63 open ocean deadtime for Landsat 8 Earth imaging approaching Hawaii

Based on row collection times for a Path 63 overpass of Mauna Loa

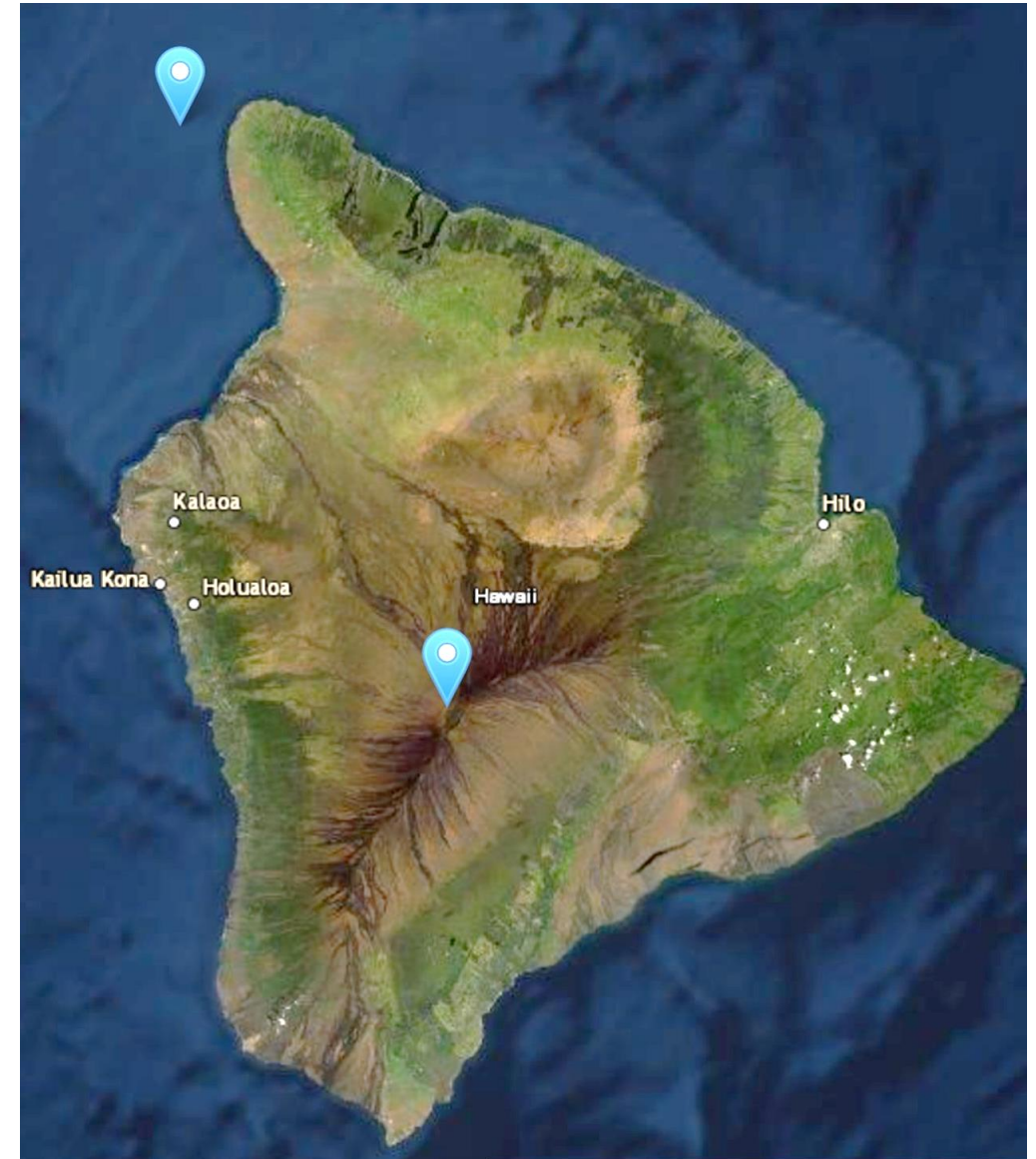
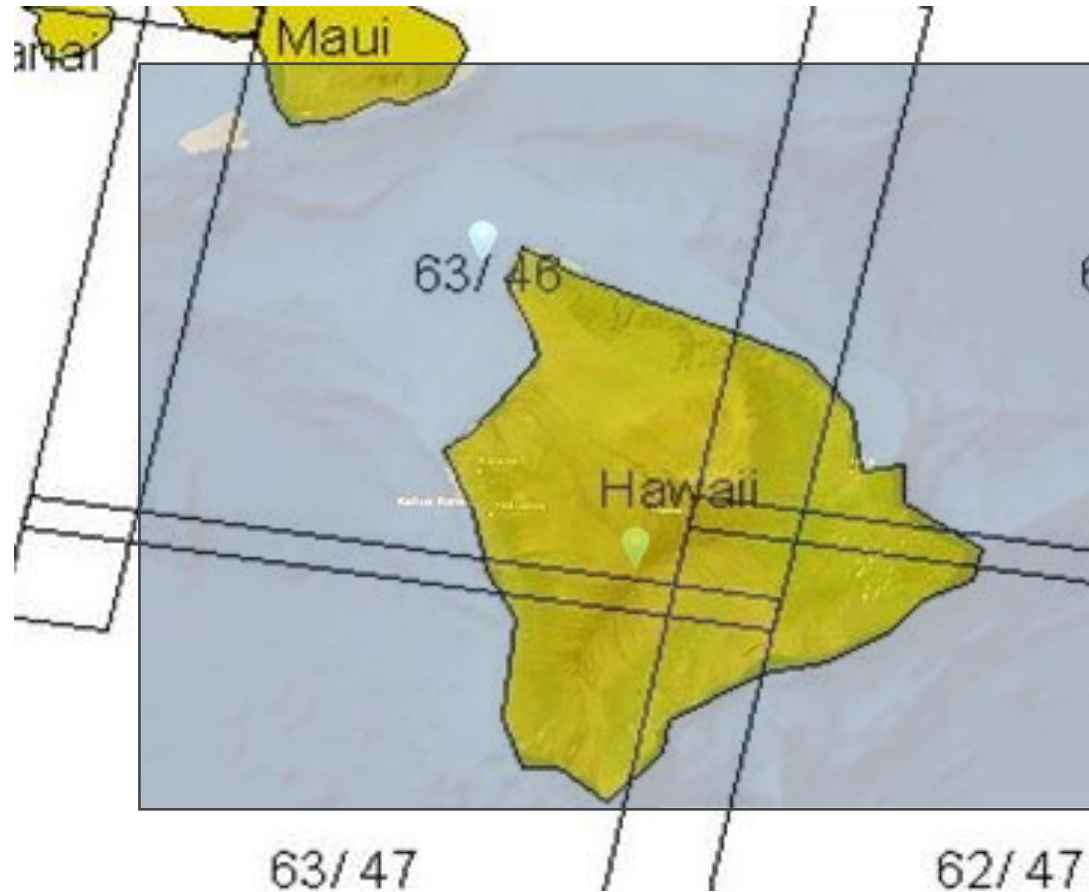
Earth imaging is not nominally processed for the period of time from the end of row 18 and the start of Row 46 during the Landsat 8 approach to Hawaii

This provides sufficient time for a shutter and lamp state collect (>10 min)



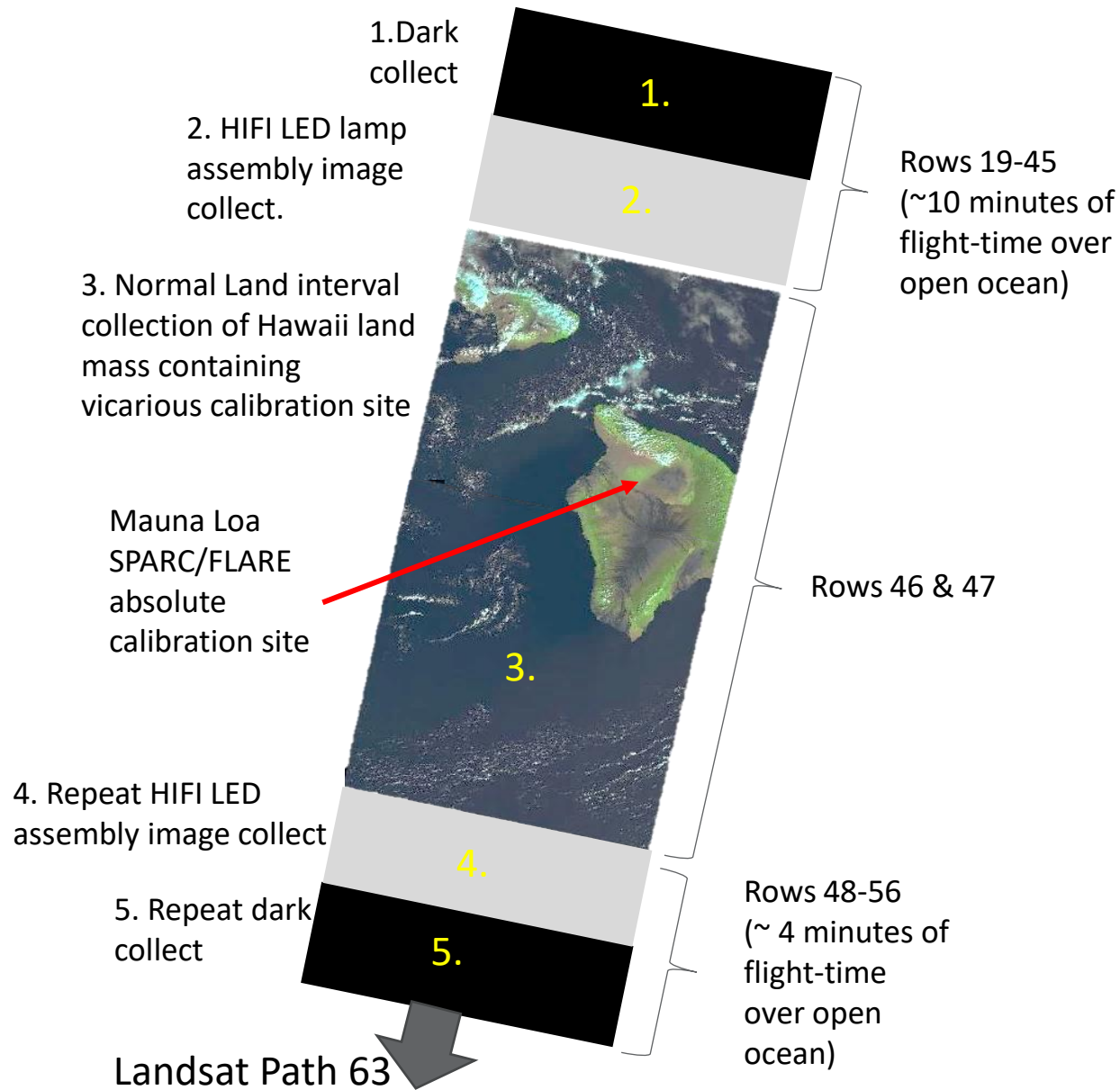


# Location of Mauna Loa FLARE site relative to path/row boundaries



Path/Row 63/46 is the nominal location of the proposed Mauna Loa FLARE site for vicarious calibration of Landsat 8 and 9 to be used in this study.

# IRIS-V method collection ConOps for re-calibration of onboard lamp system



This illustration outlines the ConOps for future Landsat systems using the IRIS HIFI calibrator (with FLARE) making use of shorter calibration collection times compared to the Landsat 8 and 9 on-board calibration systems.

The IRIS-V methodology is being tested to the degree possible with the Landsat 8 and 9 on-board incandescent lamp subsystem.

USGS ground system has determined that outside family lamp collects are too risky for current Landsat platforms

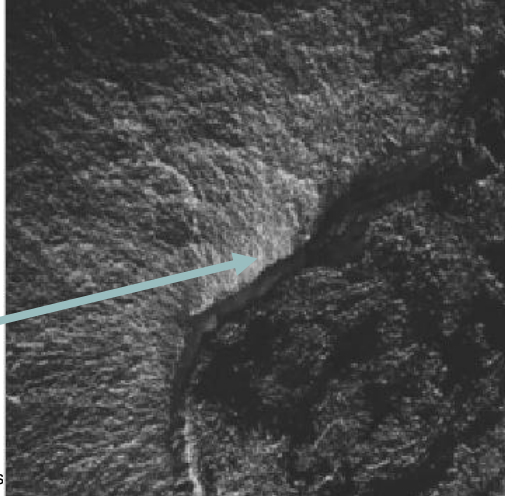
For Landsat 8 and 9, test of IRIS-V lamp collects are restricted to nominal collects over the poles once each day.

However, USGS has offered to perform the operational lamp collects at the poles before and after descending Path 63 occurs.

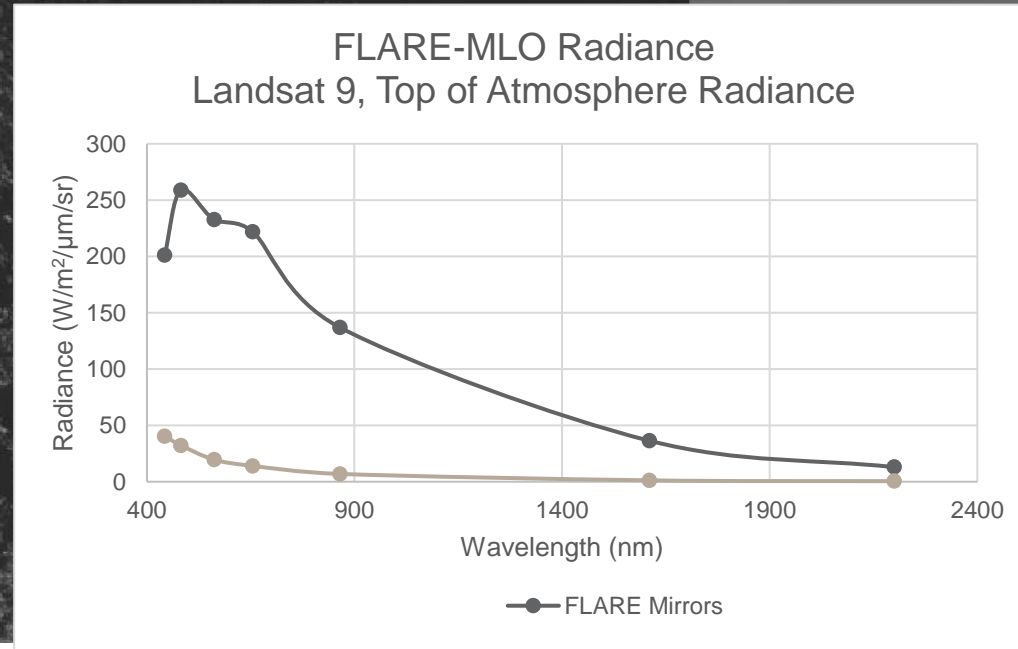
# FLARE @ MLO provides an ideal high altitude dark background site



Mauna Loa  
Caldera with  
Snow



MLO



FLARE  
SIGNAL

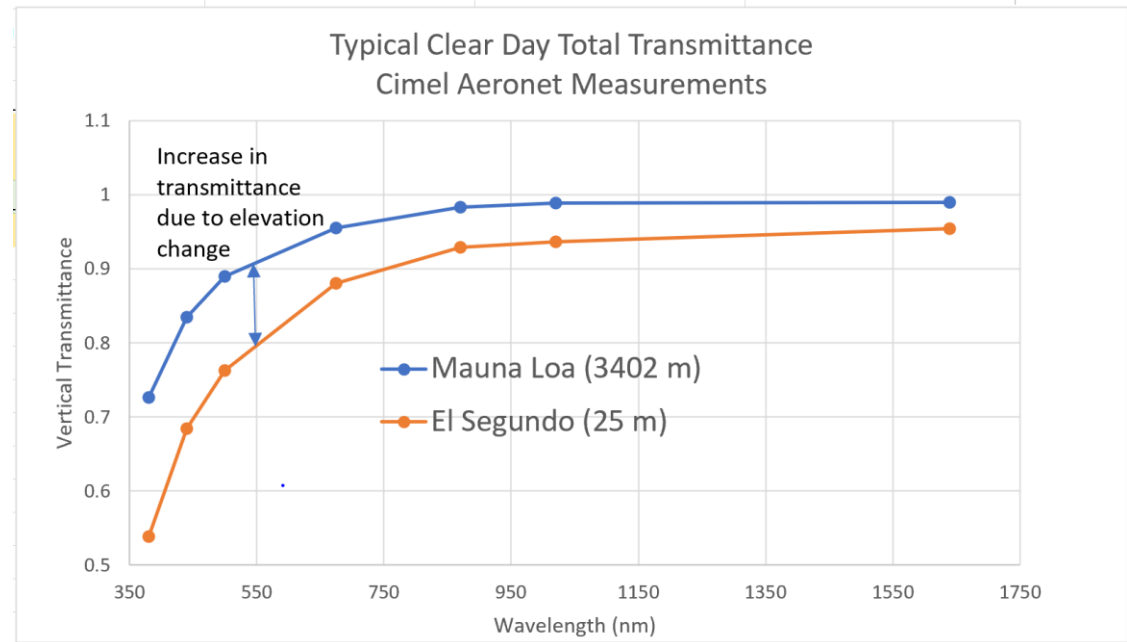
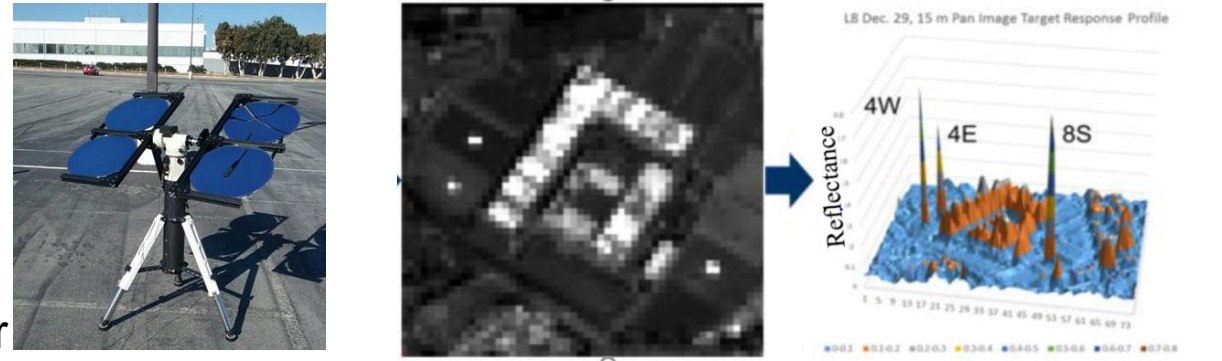
# MLO high elevation significantly improves at-sensor radiance accuracy

Better than 3% reproducibility in predicted at sensor radiance has been demonstrated at the Raytheon El Segundo SPARC test site (sea level) using multiple targets. 3-5% using a single target.



SPARC radiative transfer accuracy is dominated by uncertainty in atmospheric transmittance (all other atmospheric contributors subtract out)

Transmittance accuracy knowledge will be significantly improved with MLO FLARE operations



**FLARE < 2% absolute at-sensor radiance uncertainty should be achievable from MLO**

# Estimated uncertainty In a FLARE target vicarious at-sensor radiance prediction when deployed at MLO

Based the SPARC at-sensor radiance equation, the RSS uncertainty in the at-sensor radiance of a single SPARC target reference is):

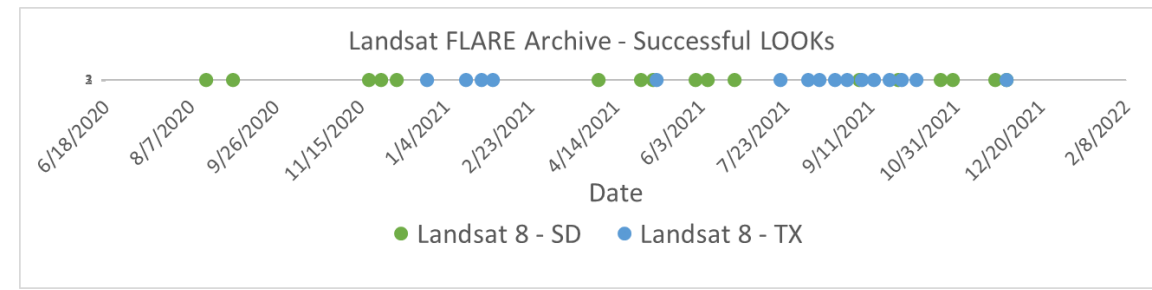
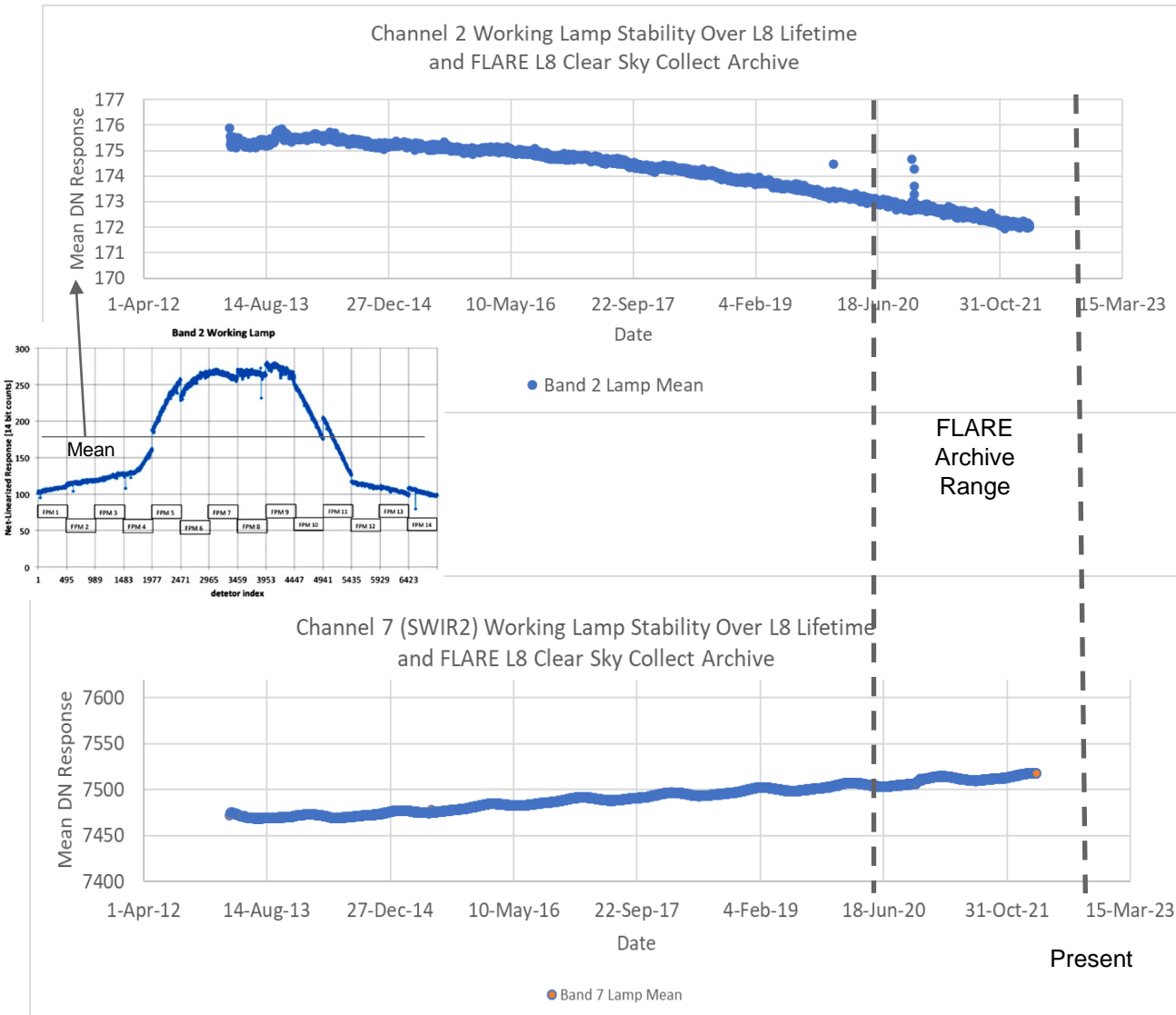
$$\frac{\delta L}{L}(SPARC) = \sqrt{\left(\frac{\delta \rho}{\rho}\right)^2 + \left(2 * \frac{\delta \tau}{\tau}\right)^2 + \left(\frac{\delta E_o}{E_o}\right)^2 + \left(2 * \frac{\delta R}{R}\right)^2 + \left(2 * \frac{\delta GSD}{GSD}\right)^2}$$

Assuming clear sky conditions at 0.55 microns the estimated uncertainty is calculated

| Symbol                               | Parameter  | % Uncertainty       |
|--------------------------------------|--|---------------------|
| $\rho$                               | Mirror Reflectance (in the field)  | 0.5%                |
| $\tau_{\downarrow}, \tau_{\uparrow}$ | Measured and Modeled Atmospheric Trans. (estimated from MLO Aeronet station data)                          | 0.8%                |
| $E_o$                                | In-band Top-of- Atmosphere Solar Irradiance (Abs uncertainty for TSIS-1 on ISS, Rel for solar variability) | 0.3% Abs., 0.2% Rel |
| $R$                                  | Mirror Radius of Curvature   | 0.25%               |
| $GSD$                                | Pixel Projected Ground Sample Distance   | 0.5%                |
| $L$                                  | Absolute At-Sensor Radiance  | RSS total 2.0 % Abs |

This value represents the at-sensor radiance uncertainty for a single target in a single image. Adding more targets in the scene will, in principle, reduce the net uncertainty and improve the performance knowledge of the sensor.

# Landsat data for IRIS-V study



These plots show the IAS lamp cal response data and the FLARE Landsat 8 collects available for this study and under analysis

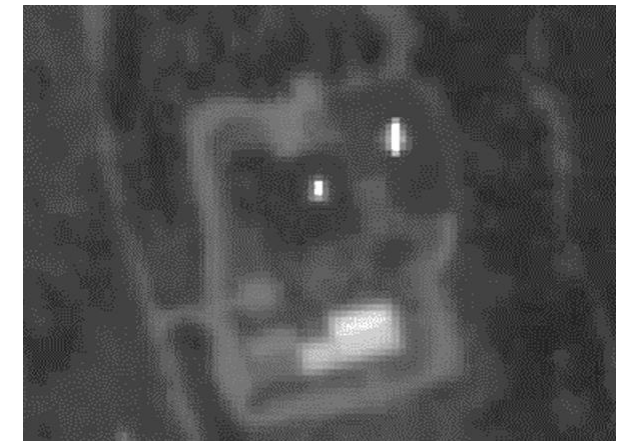
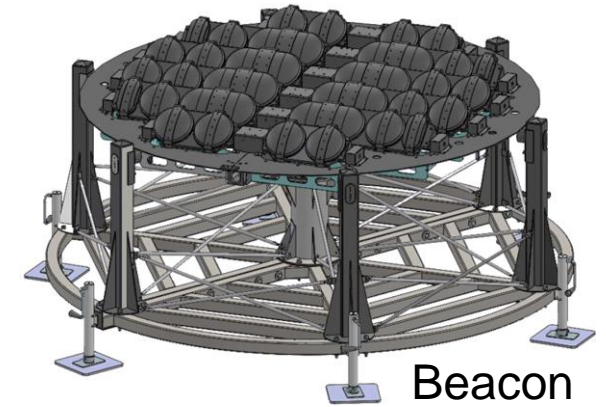
**Resulting IRIS-V Capability**

**Each Lamp cal, converted to radiance, allows stability and repeatability trending of each detector, SCA and full focal plane for each band relative to the traceable FLARE absolute radiometric scale**

**With the IRIS-V lamp calibration, the lamp source provides on-board on-demand FLARE based absolute radiometric scale calibration and validation supporting nominal daily land imaging and off-nadir maneuvers**

# IRIS-V progress summary

- FLARE calibration collects of Landsat 8 and 9 at the current South Dakota and Texas sites are continuing
- Gain coefficient analysis from the L8/9 FLARE archive is underway
- Clear sky test deployments of the portable SPARC targets in Hawaii have been completed demonstrating the high altitude and dark background performance
- Mean lamb response data processed by the Landsat Image Assessment System for lamp cals temporally closest to FLARE events, will continue to be collected through the EROS data center
- Relative trending analysis and repeatability between the lamp response and FLARE calibration will be performed to determine the IRIS-V uncertainty budget and performance applied to L8 and L9
- The process is proceeding toward moving the FLARE Beta system from Texas to MLO as well as a Lantern FLARE target (allowing a two-point cal) in 2023



Two-Point FLARE<sup>23</sup>

# The Raytheon/FLARE Team

**Dr. Jeff Puschell**, Chief Scientist Space Systems

[jjpuschell@raytheon.com](mailto:jjpuschell@raytheon.com) C: 310-503-3412

**Dr. Stephen Schiller**, Principal Calibration Scientist,

[stephen.j.schiller@raytheon.com](mailto:stephen.j.schiller@raytheon.com) C: 626-664-5577

**Chris Durell**, FLARE Business Development –

[cdurell@labsphere.com](mailto:cdurell@labsphere.com) C: 858-414-1885

**Dr. Brandon Russell**, FLARE Science Lead –

[brussell@labsphere.com](mailto:brussell@labsphere.com) C: 203-241-7253

**Will Arnold**, FLARE Program Manager –

[warnold@labsphere.com](mailto:warnold@labsphere.com) C: 603-729-7191

...